



## OPEN Mechanical characteristics of herbaceous plant root system and slope stability research

Shilin Tan<sup>1</sup>, Guoping Xiang<sup>1,2✉</sup>, Xiangning Xu<sup>1,2</sup> & Tao Liu<sup>1</sup>

It is of great significance to study the mechanical properties of plant roots and root-soil interactions on the effect of root consolidation. In order to study the mechanical effects of herbaceous plant root systems on the slopes of the Haizhou open-pit mine, *Medicagosativa L.* (Species 1), *Iris lactea Pall. var. chinensis (Fisch.) Koidz.* (Species 2), and *Euphorbia hypericifolia L.* (Species 3) were taken as the research objects to carry out indoor root tensile tests, in situ shear tests, quantitatively calculated the additional cohesive force of the root system with Wu and FBM models, compare the applicability of the two models, and the Wu model was modified to compare the soil consolidation effects of different plant root systems; A simplified slope numerical model was used to investigate the shallow damage protection effect of rooted slopes with the same root area ratio. The results showed that (1) the tensile strength of the root systems of the three herbaceous plants increased with the root diameter in a power function relationship, and the tensile strength decreased with the root diameter in a power function relationship; (2) The Wu modification coefficients of Species 1, Species 2, and Species 3 were 0.17, 0.15, and 0.58, respectively. Comparing the modification coefficients of the three herbaceous plants, Species 3 had the largest modification coefficients; Species 1 was the second largest, and Species 2 had the smallest modification coefficients; the actual increment in cohesive force was close to that in the FBM model, and the FBM model was significantly better than the Wu model; (3) The mechanical and morphological properties of Species 3 made its root system consolidation effect the greatest compared with Species 1 and Species 2 root-soil interaction.

**Keywords** Slope stability, Shear test, Wu and FBM models, Mechanical properties of root system, Root area ratio, Root soil complex

Mining, road construction, water conservancy, civil engineering, and other engineering construction produce many artificial slopes. The occurrence of slope landslides, mudslides, and other geologic disasters cause huge property losses and, at the same time, produce large-scale soil erosion. Engineering slope protection can effectively prevent and control slope disasters. However, the construction cost is high, life is limited, and visual gray pollution, ecological imbalance, etc. are caused. Plant slope protection can inhibit topsoil erosion, prevent shallow landslides, and reduce water loss, but it also has the advantages of low construction and maintenance costs and high social and ecological benefits. Plant protection alone or with engineering slope protection for slope protection has become the direction of development, and the plant root system is the basis of plant slope protection. The shallow herbaceous root system and soil interact to form a root-soil complex, which improves the shear strength of the soil body, and the shallow and deep root systems work together to restrain the deformation of the soil body and increase stability. Numerous plant root systems intertwine to form a dense cover layer to prevent soil erosion<sup>1,2</sup>. Mechanical models can be used to quantify the reinforcing effect of plant roots on the soil body. There are currently three major mechanical models for root enhancement of soil shear strength, i.e., WWM<sup>3,4</sup> (from now on referred to as Wu), FBM<sup>5,6</sup>, and RBM<sup>7</sup> models, with the more refined model being the RBM model.

Although the Wu and FBM models are not the most advanced, their parameters are easier to obtain and simpler to calculate, so many scholars widely use the model<sup>8–13</sup>. L. J. Waldron<sup>3</sup> and T. H. Wu<sup>4</sup> proposed the WWM model that plant roots' mechanical properties affect soil shear strength. However, the model assumes that all the roots in the root-soil composite fracture at the same time when it is subjected to shear, while the actual situation is that there are differences in the moments and durations of the fracture of each root, so the model overestimates the ability of the root system to increase the shear strength of the soil body of the slope<sup>8</sup>. Pollen

<sup>1</sup>The 2nd Geological Brigade Of Sichuan, Chengdu 610041, China. <sup>2</sup>Chengdu University of Technology, Chengdu 610000, China. ✉email: xiangguoping1989@163.com

and Simon<sup>5</sup> proposed and validated the root-soil interaction fiber bundle model (FBM), which can reflect the complete situation damage process of root damage by force in soil<sup>14</sup>. During the gradual increase of load in the FBM model, the weakest root breaks first, and the load it bears is equally distributed by the remaining roots, and so on, until the last root breaks, which can more realistically reflect the root-soil interactions<sup>8</sup>. Schwarz et al.<sup>7</sup> proposed the RBM model based on the FBM model, which has more considerations but does not apply to herbaceous plants<sup>15</sup>. When calculating the enhancement effect of the root system on soil shear strength, the RBM model thoroughly considered the influence of the strength of the root system in the soil, the friction between root and soil, and other related parameters on the soil shear strength, including the complete stress-displacement relationship curve including the residual stress of the root system after reaching the peak load. However, the evaluation of the correlation between root tensile strength and slope stability assumed the absence of root-soil interaction, which exists<sup>7</sup>. The Wu and FBM models can be used to calculate the additional cohesive force of herbaceous plant root systems, thereby obtaining the root system's mechanical properties and the root-soil complex's shear properties, which are essential for studying the root fixation effect on slopes. They can be simulated to quantitatively determine the effect of root fixation<sup>16–18</sup>. In order to study the mechanical effect of the herbaceous root system on slopes of the Haizhou open-pit mine, Species 1, Species 2, and Species 3 were taken as research objects, indoor root tensile tests and in situ, shear tests were carried out, the Wu and FBM models quantitatively calculated the additional cohesive force of the root system, and the applicability of the two models was compared. The Wu model was modified to analyze the mechanical properties of the root systems of different plants and to compare the effect of soil fixation on the root systems of different plants. A simplified slope numerical model was used to investigate the shallow damage protection effect of rooted slopes with the same root area ratio. The research results provide empirical guidance and practical significance for improving the stability of mine slopes in herbaceous plants. A schematic diagram of the plant-cemented slope is shown in Fig. 1.

## Materials and methods

### Experiment material

The test soil and root system originated from the northeast corner of the north gang of Haizhou open-pit coal mine in Fuxin City, Liaoning Province, with the location center coordinates of 121°41'1.58"E longitude and 41°59'57.44"N latitude, and an elevation of 143 m. The test soil and root system are from the northeast corner of the north gang of Haizhou open-pit coal mine in Fuxin City, Liaoning Province. Species 1 belongs to perennial herbaceous plants with thick and robust roots that penetrate deep into the soil layer, and it is often the plant of choice for soil and water conservation and soil stabilization on slopes<sup>19</sup>. Species 2 is because of its dense clumping, well-developed root system, resistance to cold and drought, waterlogging, saline and alkaline, trampling, barrenness, resistance to pests and diseases, and can adapt to a wider range of ecological environments. It is an excellent plant for soil improvement and maintenance of slope stabilization<sup>20</sup>. Species 3 belongs to the annual herbaceous Euphorbiaceae, *Euphorbia* spp. The study area is an open-cast coal mine, and the seeds of this plant may have been brought by coal trucks and adapted to the local climate. The root systems of the test plants were all Species 1, Species 2 and Species 3 in the field in the study area, and all of them were grown in the same place. The slope gradient of the area where the plants were grown was approximately 37°. For the control variable, the three herbaceous plants sampled were all fresh, rooted plants with the same growing

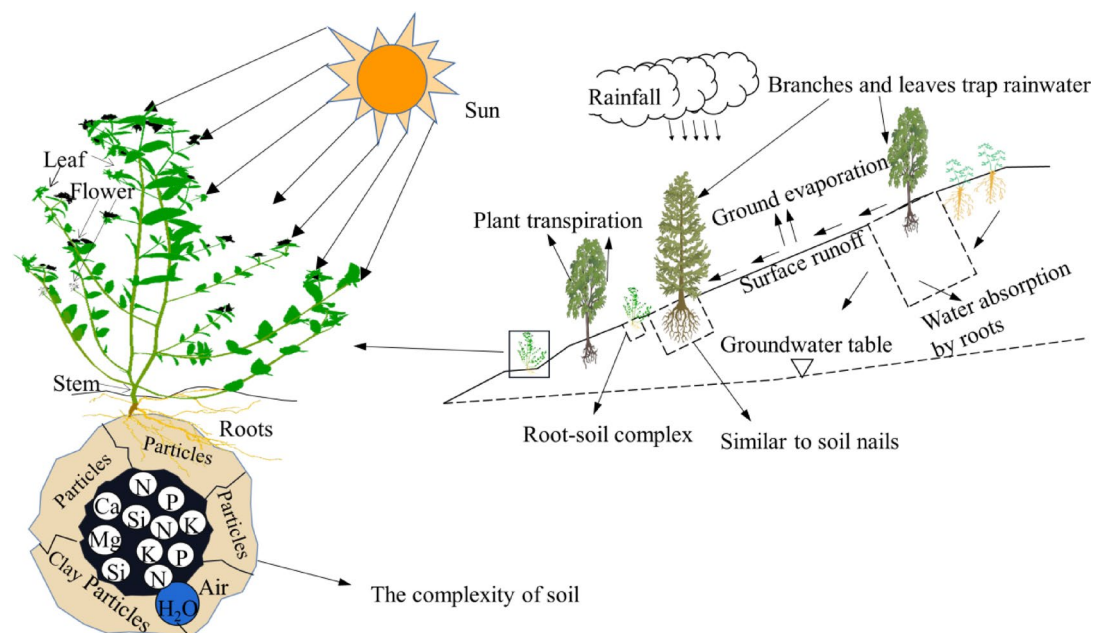


**Fig. 1.** Schematic diagram of plant soil consolidation slope protection.

environment, exhibiting normal growth, and free from pests and diseases. All had a 6-month growing cycle. The foam was added to the inside of the root collection box to avoid damage to the roots during transportation. The plants were excavated using the whole-plant excavation method, and each plant was excavated as eight plants. After excavation, the soil samples on the surface of the root system were rinsed with water and air-dried on absorbent paper for immediate testing, and part of the root system was used for tensile strength determination; the other part was used for the root-soil composite shear test. The unfinished test root systems were kept fresh in a refrigerator at 4 °C, and the tests were completed within 7 d. The root systems were dried on absorbent paper immediately after the tests. Both Species 1 and Species 3 consisted of a main root and lateral root; there were many fine roots on the main root and lateral root, the main root system was large, the lateral root system was small, Species 1 had fewer fibrous roots, and tomato Species 3 had more fibrous roots, and Species 1 root system was straighter. In contrast, the tomato Species 3 root system had more curved roots. Species 1 has a fast growth rate, a strong root system, and strong adaptability to the environment of soil samples in the study area. It can quickly form a root system in the shallow soil layer to achieve the strength and depth of soil consolidation and slope protection. The large number of fibrous roots and curved morphology of the root system of Species 3 is favorable for fully absorbing water and nutrients, which also makes the contact area with the soil larger, and the effect of soil consolidation is better. The root morphology of the three herbaceous plants is shown in Fig. 2.

Surface soil was obtained at the plant growth site. The soil bulk weight was 1.32 g/cm<sup>3</sup> by the ring knife method, the soil pH was 8.41 by the pH method, the liquid limit and plastic limit were 29.25% and 19.39%, respectively, by the combined liquid-plastic limit method, the moisture content of the soil was 15% by the drying method, and the maximum dry density of the soil was 1.889 g/cm<sup>3</sup> by the percussion test. The sieve method measured the soil particle gradation of > 5.00, > 2.00 to 5.00, > 1.00 to 2.00, > 0.50 to 1.00, 0.25 to 0.50, 0.074 to 0.25, and < 0.074 mm particles accounted for 8.46%, 15.24%, 10.78%, 10.02%, 17.78%, 31.05% and 6.67%, respectively.

## Experiment method

### Root tensile test

Tensiometer by Aigu zp-500 digital display push-pull tensiometer, by the fixture, tension frame, electronic digital display tensiometer, signal collection device, etc., range displacement of 500 N, accuracy  $\pm 0.1$  N; measure root diameter and root length of the vernier caliper for the electronic digital display vernier calipers, range of 150 mm, accuracy  $\pm 0.01$  mm. Three kinds of plants were selected: several whole plants with different root diameters of the root system, with scissors to cut them unbroken; the length of the root segments with no damage, small bending amplitude, and small changes in root diameter were (100  $\pm$  5) mm, and several single roots with different root diameters were prepared as a group for single-root tensile test, and the difference in the diameter of the two ends of the root segments should be within 0.3 mm, and those exceeding the difference should be discarded. For each plant root system, 100 groups were prepared. Due to the stress concentration effect in the contact position between the fixture and the root, it is easy to fracture the root in the part near the fixture during the test due to clip breakage or root skin peeling, so sandpaper was glued to the fixture jaws to reduce the root skin peeling or the specimen being clipped off.

The vernier calipers measured the diameters of the two ends of the prepared root segments and three positions in the middle. The average value was taken as the root diameter of the root segments, which was recorded, and then the root segments were fixed on the digital push and pull tensiometer. The fixtures fixed the two ends, and the length of the fixed root was 1 cm. The test root segments were 8 cm. After the root segments were fixed, the tensiometer was zeroed, and the pulleys were evenly rotated (the speed was 10 mm/min) until the roots were pulled off. The maximum pull force was recorded in the course of the tensile damage. The maximum tensile force was recorded during tensile damage. Changes in root length and tensile strength of some root segments were recorded during tensile damage to determine the changes in root stress with strain. In order to ensure the accuracy of the data, the test of root breakage due to pinching off or root skin detachment near the fixture part was regarded as a failure, and only the data of root breakage at the position of 1/3 to 2/3 were retained. The tensile strength was calculated using the formula<sup>21</sup>:

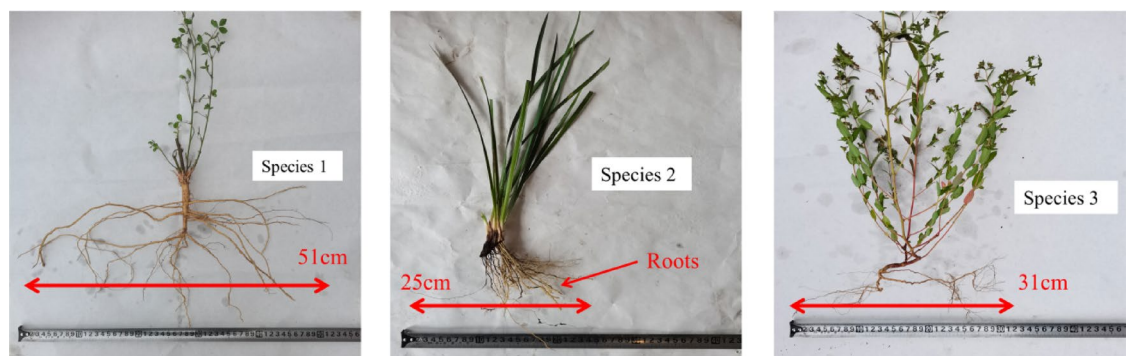


**Fig. 2.** Morphological distribution of the three herbs.

$$T = \frac{4F}{\pi d^2} \quad (1)$$

Where:  $F$  is the tensile force (N),  $d$  is the root diameter (mm),  $T$  is the tensile strength (MPa).

From Hooke's law, the material in the unidirectional stress state, the stress is proportional to the strain:

$$E = \frac{\sigma}{\varepsilon} \quad (2)$$

Stress  $\sigma = T$  (MPa), strain  $\varepsilon = \Delta L/L$ , elongation;  $L$  is the length of the root section (cm), all 10 cm;  $\Delta L$  increase in root length after tension (mm); and  $E$  modulus of elasticity (MPa).

#### *Design of in situ soil extraction shear tests*

The original sampling soil shear test device is shown in Fig. 3; the shear system mainly consists of the upper and lower straight shear box, the upper box cover, the baffle plate, and the guide rail, the total height of 200 mm of which the upper box is 100 mm, the lower box is 100 mm, the material of the box body is a 5 mm thickness of the PVC board, the box body internal polishing and sanding. The lower straight shear box is fixed on the ground with the steel base plate through bolts, and the lower straight shear box is fixed during the whole straight shear test. Between the upper and lower straight shear box, steel balls were placed on the wall of the box in the sliding direction, and there was a groove in the sliding direction of the lower box wall so that it could be put into the steel balls. A stopper is mounted outside the lower box wall to prevent the upper box from slipping sideways during shearing, thereby preventing it from sliding out of the steel balls. The shearing device was fabricated according to the literature<sup>12</sup>.

During the test, the upper box cover is used solely to compact the soil to its natural state of tightness, similar to the shearing process. There is no upper box cover to ensure that the condition of its shear is within the natural condition. In the test, upper box horizontal movement thrust directly from the dynamometer is conducted as far as possible to make the horizontal thrust gauge thrust line of action close to the centerline of the shear seam. At the test end of the thrust gauge, a very stiff steel head is installed so that it acts directly on the bottom of the upper box, and a steel bar is placed on the bottom of the upper box so that all of its thrust acts as close as possible to the centerline of the shear seam. The thrust gauge is mounted on a horizontal support with a rotating wheel, and the displacement pushed by the gauge is 1 mm for one revolution of the wheel. When the shear test is over, use vernier calipers to measure (accuracy of  $\pm 0.01$  mm) the root diameter on the shear surface and record the root position; use a 64-megapixel camera to photograph the root morphology distribution map of the soil profile and import it into the Adobe photoshop CS6 software to get the changes in the root area ratio at different depths based on the conversion relationship between the root diameter and the scale of the ruler. The root-soil complex shear tests were all repeated three times, and the cohesive force was averaged.

#### **Calculation of additional root cohesion**

##### *WWM model*

Waldron<sup>3</sup> and Wu<sup>4</sup> proposed the Wu model for enhancing the shear strength of soil by mechanical properties of plant roots, in which the increment of shear strength is closely related to the tensile strength of the root system. The increment of shear strength is calculated with reference to Eq. 3.

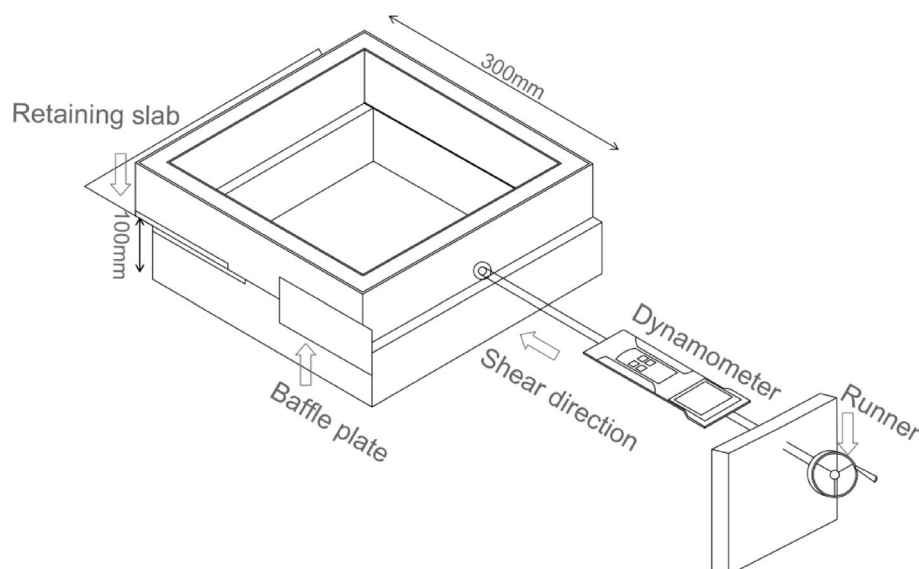


**Fig. 3.** In-situ shear test setup.

$$\Delta S = 1000T_N(RAR)(\sin \theta + \cos \theta \tan \varphi) \tag{3}$$

Where:  $\Delta S$  is the soil shear strength increment (kPa) induced by the root system of the soil for the root perpendicular to the shear surface,  $T_N$  is the average tensile strength of the root system (MPa),  $\varphi$  is the effective internal friction angle of the soil ( $^\circ$ ),  $\theta$  is the bending angle of the root system in the process of shear ( $^\circ$ ), and  $RAR (A/A_s)$  is the ratio of the cross-sectional area of the root system to the root-soil shear surface area, which is known as the root-soil area ratio<sup>11</sup>. The force diagram of the vertical shear surface of the root system is shown schematically in Fig. 4, where  $h$  is the width of the shear zone (mm),  $x$  is the horizontal displacement of the root system (mm), and  $\tau_r$  is the friction between the root-soil composite (N).

When the root system is perpendicular to the shear surface, Wu et al.<sup>4</sup> concluded that the variation interval of  $(\cos\theta \tan\varphi + \sin\theta)$  values when the shear deformation angle  $\theta = 40^\circ$  to  $70^\circ$  and the internal friction angle  $\varphi = 25^\circ$  to  $40^\circ$  of the root-containing soil body varies within the range of 0.92 to 1.31 and will take the average value of 1.2. After unifying the units, the increase in shear strength of the root-soil complex provided by the root system in the Wu model is simplified to Eq. 4.

$$\Delta S_{WWM} = 1200T_N RAR = 1200T_N \frac{A}{A_s} = R_f \sum_{i=1}^n \frac{F_i}{A_s} \tag{4}$$

Since the fracture of the root system during shear is a process from fine to large roots, which transforms the tensile force of the root system itself into the friction force at the root-soil interface, and since eventually, the main root may not fracture, resulting in a higher increase in shear strength than the measured value obtained by using this model<sup>13</sup>, a correction factor,  $k_s$ , was introduced.

$$\Delta S_1 = k_s \Delta S_{WWM} \tag{5}$$

$\Delta S_{WWM}$  model the cohesive force of root-increased soil obtained from theoretical calculations, and  $\Delta S_1$  is the cohesive force of root-increased soil obtained from experiments. Corresponding herbaceous amendment parameters were obtained based on their ratios. The model's main parameters affecting root soil consolidation are the root area ratio  $RAR$ , the average tensile strength  $T_N$ , and the correction coefficient  $k_s$  of the model.

$$k_s = \frac{\Delta S_1}{\Delta S_{WWM}} \tag{6}$$

The root area ratio was calculated using the ratio  $A_s$  of the total root cross-sectional area  $A$  at the shear to the cross-sectional area of the soil, using the formula:

$$RAR = \frac{A}{A_s} = \sum_{i=1}^n \frac{\pi n_i D_i^2}{4A_s} \tag{7}$$

Where:  $RAR$  is the root area ratio;  $n$  is the number of roots in the shear surface ( $n$ ).

*FBM model*

There exist three ways of force allocation in the FBM model. They are allocation by root area, allocation by root diameter and allocation by root number<sup>6</sup>. Mao Z et al.<sup>6</sup> considered the root number approach for allocation as more advanced. Assuming the presence of roots in a given soil block, the area of the block is denoted as  $A$  and the total number of roots is denoted as  $N$ <sup>22</sup>. The roots are ranked according to their tensile strength (i.e., strongest to weakest are roots numbered 1 to  $N$ ). For the  $n$ th root among them ( $1 \leq n \leq N$ ),  $A_n$  denotes the diameter of the root; denotes the cross-sectional area of the root;  $RAR_n = A_n/A_s = \pi D_n^2/4A_s$ ; and  $T$  denotes the tensile strength. During loading, when one or more roots break, the force on their roots is carried by the remaining roots. When root  $j$  breaks, the effect of root reinforcement can be characterized by Eq. 8:

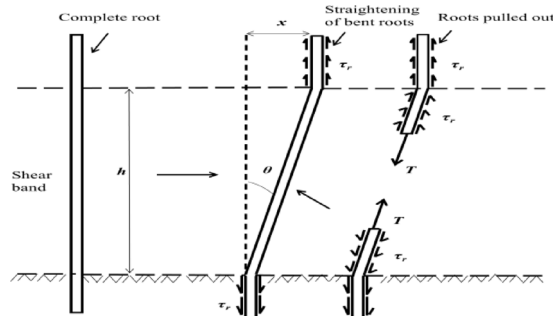


**Fig. 4.** Schematic representation of forces bearing roots perpendicular to the shear surface.

Soil types	Densities kg/m <sup>-3</sup>	Modulus of elasticity /MPa	Poisson's ratio	Cohesion /kPa	internal friction angle/°	Tensile strength/kPa
Loam layer	1320	5	0.25	8.28	17.8	0
Vein of ore	1860	50	0.35	4.98	35.8	2.0

**Table 1.** Model parameters.

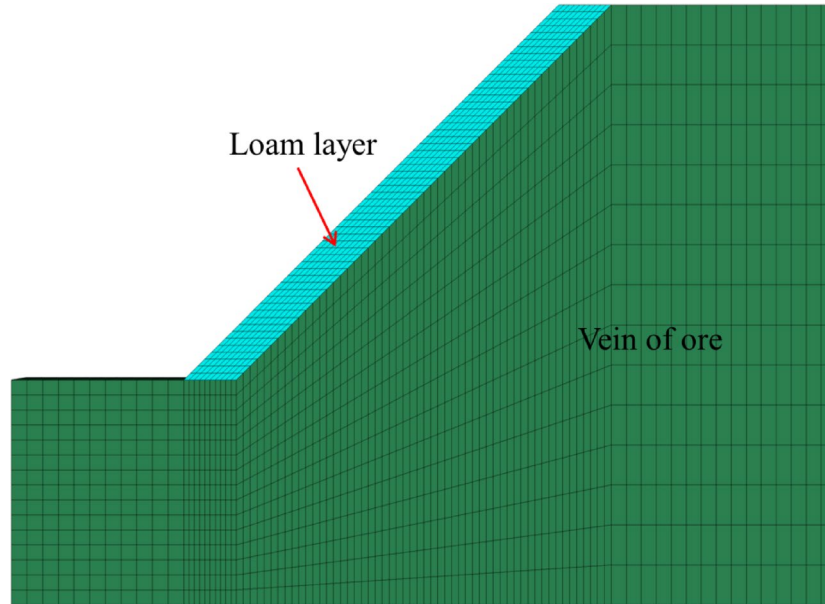


**Fig. 5.** Schematic diagram of the side slope.

$$\Delta S = 1000R_f \frac{F}{\sum_{n=1}^j ((\pi/4)D_n^2)} \sum_{n=1}^j RAR_n \tag{8}$$

Where 1000 is the conversion constant from MPa to kPa and is the root orientation factor. In order to compare the WWM model, the root orientation factor is taken as 1.2, concerning the literature<sup>4</sup>. Distribution by the number of roots when the fracture occurs at root *j*, it is calculated concerning Eq. 9.

$$\frac{\pi}{4} D_j^2 T_j = \frac{F}{j} \tag{9}$$

Bringing Eq. 9 into Eq. 8 yields:

$$\Delta S = 1000R_f T_j \frac{(\pi/4)D_j^2 j}{A} = 1000R_f T_j RAR_j j \tag{10}$$

The increment of cohesion due to the distribution by the number of roots by the FBM model is:

$$\Delta S_{FBM} = 1200 \times \max(T_j RAR_j j) \tag{11}$$

**Slope calculation model and parameters**

Soil was collected from the plant growth area. Soil samples were taken from the mineral and guest soil layers (rootless soil) with a ring knife (Φ61.8 mm × 20 mm). The desired soil samples (rootless soil) were taken from the loam layer and vein of ore using a ring knife (61.8 mm × 20 mm). The soil samples were taken at 0.3 and 0.6 m below the ground surface. The growth form of herbaceous plants was sampled using a paring knife to remove excess soil along the edge of the loop knife. After sampling with the ring knife, the soil was covered with the ring knife cover and sealed. Ring knife cover, sealed, and brought back to the laboratory. The soil samples were immediately analyzed in the laboratory using a balance (accuracy ± 0.01 g). Moreover, five samples were used to measure the natural density of the soil. The natural density of the soil was measured. The cohesion and angle of internal friction of the loam layer and vein of ore were obtained from the in situ soil shear test. The other mechanical parameters of the loam layer and vein of ore in the slope model are set according to the literature<sup>23,24</sup>.

This paper, FLAC3D is used to establish the herbaceous plant root reinforcement drainage field slope model, and the stability analysis is carried out. The mechanical parameters of the model are shown in Table 1, and the internal friction angle and cohesion of the guest soil layer are derived from the test, as shown in Table 1. The grid division is shown in Fig. 5. The bottom width of the slope model is 11 m, and the height is 8 m, in which the side slope is 5 m high, the slope is 45°, and the thickness of the guest soil layer is 0.5 m. The strength reduction method analyzed the slope model, and the stability analysis was carried out. The strength discount method was used to calculate the factor of safety ( $F_s$ ) for the bare soil slope and the slope with the same root area ratio of the three herbaceous plants to determine the effect of soil consolidation of different plant roots when the RAR was 0.05%, to quantify the reinforcement effect of plant roots on the slope through the factor of safety, and to provide a basis for the selection of the plant Species for slope protection. A schematic of the slope model is shown in Fig. 5. According to Eq. 12, a root area ratio of 0.05% for Species 1, Species 2, and Species 3 resulted in incremental clay cohesion in the guest loam layer of 1.781 kPa, 6.816 kPa, and 7.152 kPa, respectively.

### Test data processing

The collected data were processed and analyzed using Excel. The significance of the root diameter and its mechanical properties were fitted to a curve function and analyzed by one-way ANOVA, and plotted using the software Origin 2018.

## Results and discussion

### Experiment results

Figure 6 is used to derive the results. The root tensile strength and tensile strength of the three herbaceous Species in the study area were all related to the root diameter in a power function, with the tensile strength being positively correlated with the root diameter and the tensile strength being negatively correlated with the root diameter.

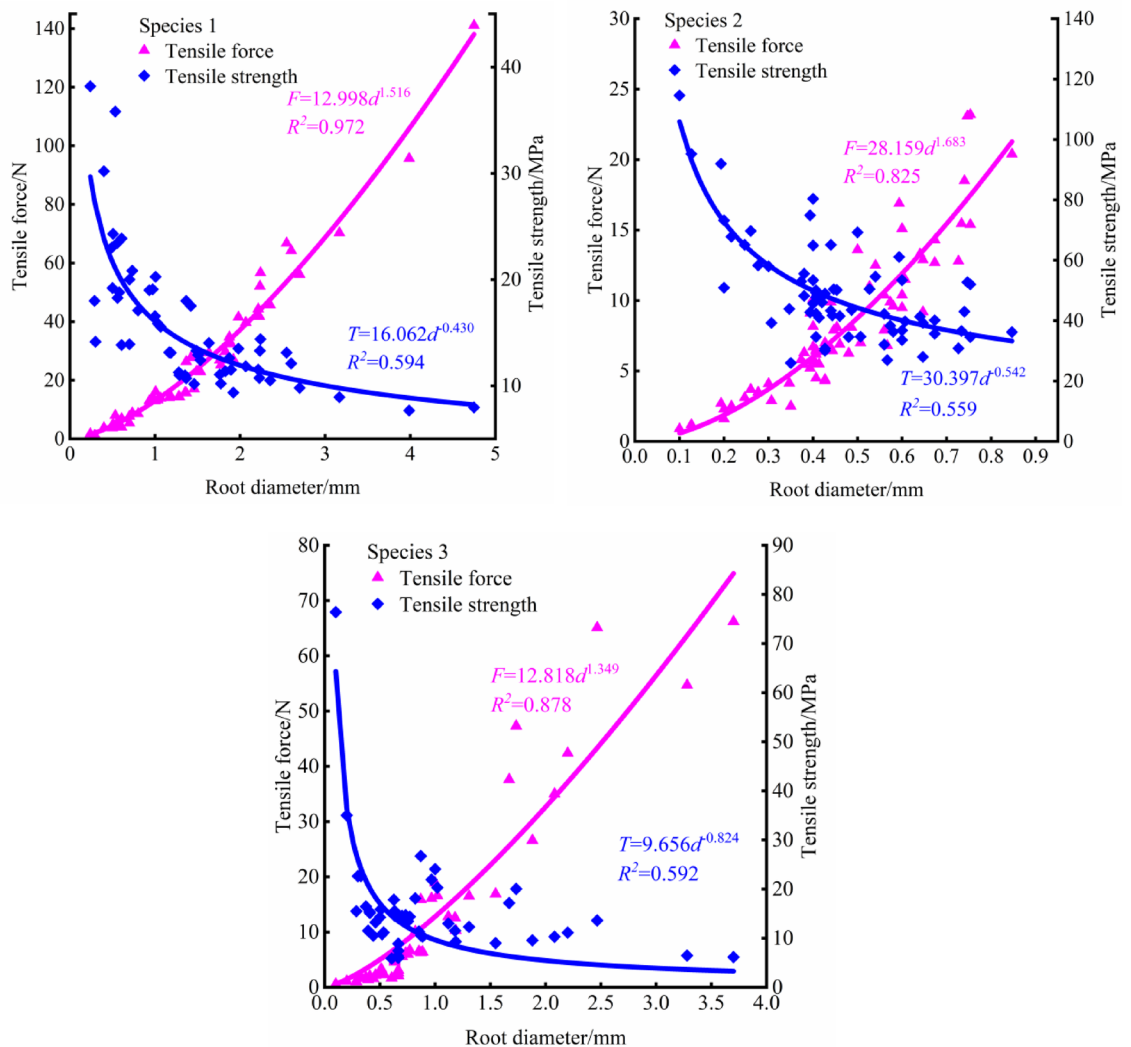


**Fig. 6.** Relationship between tensile strength and tensile strength and root diameter.

Floristics	RAR/%	$\Delta S_1/\text{kPa}$	$\Delta S_{\text{WWM}}/\text{kPa}$	$k_s$	$\Delta S_{\text{FBM}}/\text{kPa}$
Species 1	0.13	2.74	13.04	0.17	2.79
Species 2	0.019	2.59	17.25	0.15	4.63
Species 3	0.023	3.29	5.67	0.58	5.04

**Table 2.** Correction coefficient.

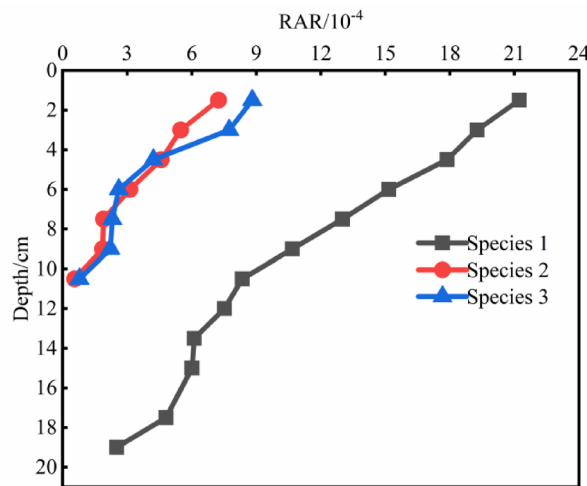


**Fig. 7.** Root area ratio varies with depth.

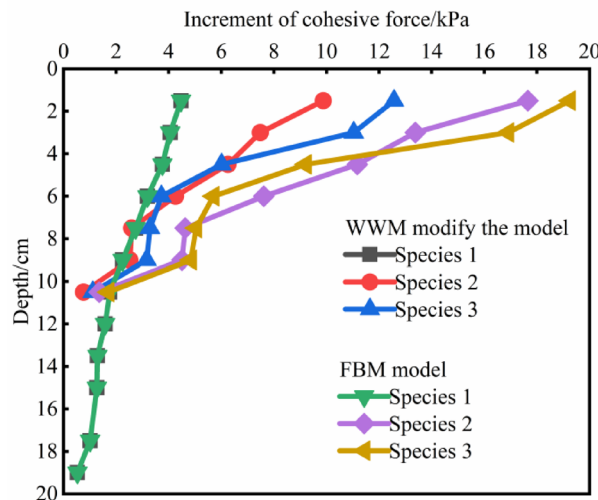


**Fig. 8.** Relationship of root additional adhesion with depth of herbaceous plants.

The experimental results are shown in Table 2; Figs. 7 and 8. The Wu correction coefficients of Species 1, Species 2, and Species 3 were 0.17, 0.15, and 0.58, respectively; comparing the correction coefficients of the three herbaceous plants, Species 3 was the largest, Species 1 was the second largest, and Species 2 was the smallest; the actual increment of cohesive force was close to that in the FBM model, and the FBM model was significantly superior to the Wu model; the root area ratio and the additional cohesive force of the root system were both reduced with the increase of the depth gradually; The increment of the additional cohesive force of root system after Wu model correction was closest to FBM model for Species 1, followed by Species 3, and the furthest difference was for Species 2 root system; Mechanical and morphological properties of Species 3 gave its root system the most significant effect on soil consolidation compared to Species 1 and Species 2 root-soil interactions.

The experimental results are shown in Fig. 10. The maximum shear strain increments of the three herbaceous shallow slopes were reduced compared to the bare slopes, and all formed circular arc-shaped slip surfaces during

instability. The upper-stress concentration phenomenon on the circular slip surface of slopes was improved, with the most obvious improvement in the shallow slopes of Species 3. The maximum shear strain increment of Species 1, Species 2, and Species 3 shallow slopes were reduced by 8.11%, 10.92%, and 13.75%, respectively, compared with the improved soil slopes, so the effect of soil consolidation of Species 3 was the most effective.

## Discussion

### *Tensile force and tensile strength as a function of root diameter*

Based on the single root tensile test, various indexes were collected and counted, including the number of successful samples in the test, root diameter, tensile force, tensile strength, and average tensile strength. The successful sample size of Species 1 was 55 groups, with root diameter ranging from 0.24 to 4.76 mm, tensile force from 1.7 to 141.1 N, tensile strength from 7.67 to 38.20 MPa, and average tensile strength of 11.33 MPa; Successful samples of the Species 2 root system were 66 groups, with root diameter ranging from 0.10 to 0.86 mm, tensile strength from 0.9 to 23.2 N, tensile strength from 26.90 to 114.60 MPa, and average tensile strength of 43.71 MPa; The success of the samples of Species 3 was 49 groups, with root diameter ranging from 0.20 to 3.70 mm, tensile force from 0.6 to 66.2 N, tensile strength from 5.88 to 76.40 MPa, and average tensile strength of 10.18 MPa. Among them, the Species 2 root test had the smallest range of root diameters and the most considerable average tensile strength. According to the results of single-root tensile experiments of the three herbaceous plants, the fitting relationship between root tensile strength and tensile strength and root diameter is shown in Fig. 6. The curvilinear regression fitting of Species 1, Species 2, and Species 3, tensile force  $F$  with root diameter  $D$ , showed a power function relationship. The functional relationship between tensile force and root diameter was,  $F = 13.009D^{1.516}$ ,  $F = 28.159D^{1.683}$ ,  $F = 12.818D^{1.349}$ , respectively. The root system tensile force increased with the increase in root diameter, which was positively correlated with the root diameter. The tensile strength obtained from the plant test was divided by the corresponding root area to obtain the corresponding tensile strength. The tensile strength  $T$  of Species 1, Species 2, and Species 3 was nonlinearly fitted to the root diameter  $D$ . The best fitting relationships were all power function relationships. The functional relationships between tensile strength and root diameter were,  $T = 16.062D^{-0.430}$ ,  $T = 30.397D^{-0.542}$ ,  $T = 9.656D^{-0.824}$ , respectively. The tensile strength of the root system decreased with the increase in root diameter and was negatively correlated with root diameter. The tensile strength properties of the root systems of the three herbaceous plants were analyzed by covariance analysis, and there were significant differences in their mechanical properties ( $P < 0.01$ ).

### *Analysis of the in situ shear test results*

The cohesion increment obtained through the test was recorded as  $\Delta S_j$ ; the cohesion increment calculated according to the Wu model was recorded as  $\Delta S_{WWM}$ ; and the cohesion increment calculated according to the FBM model was recorded as  $\Delta S_{FBM}$ , which was calculated according to the distribution of the number of roots, and the calculation was referred to Eq. 11. The results of the shear test of the original samples of the three herbaceous plants are shown in Table 2. The actual increments of cohesion of Species 1, Species 2, and Species 3 were 2.74 kPa, 2.59 kPa and 3.29 kPa, respectively, and the theoretical increments of the Wu model were 13.04 kPa, 17.25 kPa and 5.67 kPa, respectively. The theoretical increments of the FBM model were 2.79 kPa, 4.63 kPa and 5.04 kPa, respectively, and the actual increments of cohesion were closer to the increments of the FBM model, which was significantly better than the Wu model. The Wu correction coefficients of Species 1, Species 2, and Species 3 were 0.17, 0.15, and 0.58, respectively. Comparing the correction coefficients of the three herbs, Species 3 was the largest, and Species 2 was the smallest. The correction coefficients of the different herbs varied, which was attributed mainly to differences in the mechanical properties of the root system and root-soil interactions.

Considering from the perspective of the test process and root tensile properties, some roots of Species 1 were not cut during the shearing process except the primary root, and some roots were cut from the lower shear box to the upper shear box, and the fine roots tended to be cut, and the tensile strength was close to that of Species 3, but the root system had a strong resistance to deformation, which led to the number of root shear segments being less, and the root tensile performance was not given full play to, and the modification coefficient was smaller; In the Species 3 shearing process, except for the primary root, other root systems tend to shear off; the root system's tensile strength is small, deformation resistance is poor, the number of fine roots is large, the primary root system is small, resulting in the whole play of the mechanical properties of Species 3, the correction coefficient is the largest; Species 2 root system root diameter is smaller, but the tensile strength is much larger than Species 1, and through the Species 3 root system, resulting in the shear process, is the least likely to be poorly pulled, more likely to slip from the lower shear box to the upper shear box, ultimately resulting in the smallest correction coefficient. Considering the perspective of root-soil interaction, Species 1 and Species 2 root systems are elastic-plastic materials, and the root system morphology is straight, with strong deformation resistance. The friction and meshing between roots and soil are slight, resulting in the mechanical properties needing to be fully utilized in shear damage. Among them, Species 2 has the greatest tensile strength and the most substantial deformation resistance, resulting in the smallest correction coefficient; Species 3 is an elastic material with weak deformation resistance; except for adhesion between roots and soil, the bending morphology leads to considerable friction and meshing between roots and soil, resulting in its mechanical properties in the process of shear damage to give full play to the correction coefficient is the largest.

The graph of  $RAR$  of herbaceous plants with depth is shown in Fig. 7. For the same depth of root content, the Species 1 root system was larger than that of Species 2 and Species 3, and Species 2 and Species 3 were close. The  $RAR$  all decreased gradually with soil depth; the root diameter of Species 3 was smaller and had more fine roots, leading to more accurate results of the shear test; Species 1 had longer roots, larger root diameters and fewer fine roots, leading to fewer sheared roots and smaller correction coefficients; the Species 2 root system all

had smaller root diameter and no main root, and the trend of RAR change was close to that of Species 3. Based on the modified Wu and FBM model cohesion increment of the three herbaceous plants, the additional cohesion increment of the corresponding root systems at different depths was calculated, as shown in Figs. 7 and 8. The increment of root-attached cohesion all decreased with increasing depth, which was due to the root content, and the change of root content was synchronized with the change of root-attached cohesion. The trends were the same, comparing the RAR and root-added cohesion changes at the same depth. Within the range of 0–7.5 cm depth, the root content of Species 3 was less, and the root-attached cohesion was greater, indicating that the root system of Species 3 fully exerted the ability of soil consolidation and had the best consolidation capacity. The closest increment of cohesion between the modified WWM model and the increment of cohesion of the FBM model was that of Species 1, with Species 3 coming next, and the furthest difference was that of the root system of Species 2. Table 2 shows that the viscous cohesion increment corresponding to Species 1, Species 2 and Species 3 at RAR of 0.05% were 1.781 kPa, 6.816 kPa and 7.152 kPa, respectively. The calculation formula is as follows:

$$\Delta S_{0.05\%} = \frac{\Delta S_1}{RAR} \times 0.05\% \quad (12)$$

The number of bends within the root segments of the Species 1 and Species 2 root systems tested was low. The number of bends within the root segments of the Species 3 root system was high. The number of bends within the 2-cm root segments less than or equal to two can be referred to as overall bends, and greater than two is referred to as localized bends, and the delineation of the bending morphology of the root system is shown in Fig. 9. The root-soil action mechanism can be summarised as follows: with the intensification of shear damage, the root system begins to stretch, and the root system and soil interface bonding and friction gradually mobilize and transform until the root system undergoes shearing. There is bonding and friction between the curved root system and the soil body and strong meshing between the curved and undulating root system tooth ribs and the soil body<sup>25</sup>. Root-soil meshing is significantly stronger than interfacial bonding and friction<sup>25</sup>. When the relative displacement of the root-soil occurs, the interfacial bonding will be rapidly destroyed. In contrast, the meshing effect is still able to continue to play a role in significantly enhancing the shear strength of the root-soil composite of Species 3.

#### Slope stability analysis

To quantify the effect of the root system of the three herbaceous plants on slope stabilization, the maximum shear strain increment of shallow slopes at a RAR of 0.05% for the bare soil slope and the three herbaceous plants is shown in Fig. 10, and the safety coefficients of the bare soil, Species 1, Species 2 and Species 3 slopes are 1.582, 1.598, 1.645, and 1.652, respectively. The maximum shear strain increments of the three herbaceous shallow slopes were reduced compared to the bare slopes, and all formed circular arc-shaped slip surfaces during instability. The upper-stress concentration phenomenon on the circular slip surface of slopes was improved, with the most obvious improvement in the shallow slopes of Species 3. The maximum shear strain increment of Species 1, Species 2 and Species 3 shallow slopes were reduced by 8.11%, 10.92% and 13.75%, respectively, compared with the improved soil slopes, so the effect of soil consolidation of Species 3 was the most effective.

## Conclusions

- (1) Root tensile force and tensile strength of the three herbaceous plants in the study area showed power function relationships with root diameter; tensile force was positively correlated with root diameter, and tensile strength was negatively correlated with root diameter;
- (2) The Wu correction coefficients of Species 1, Species 2 and Species 3 were 0.17, 0.15 and 0.58, respectively; comparing the correction coefficients of the three herbaceous plants, Species 3 was the largest, Species 1 was the second largest, and Species 2 was the smallest; the actual increment of cohesive force was close to that

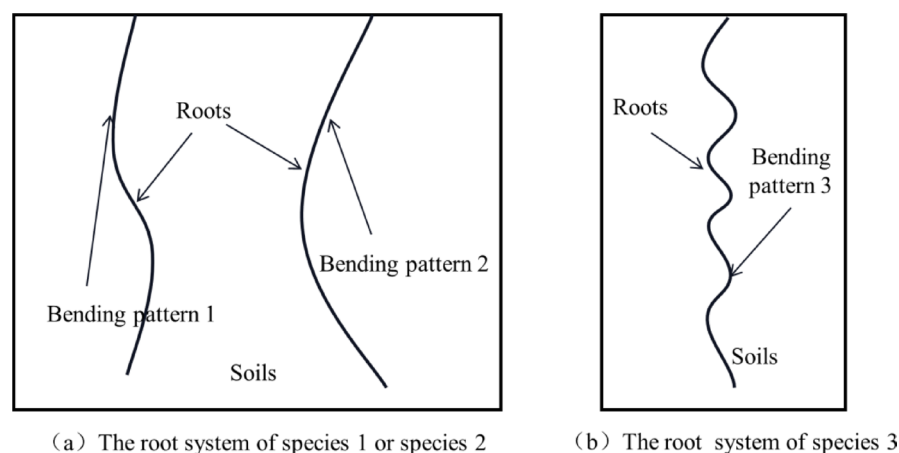


**Fig. 9.** Division of root bending morphology.

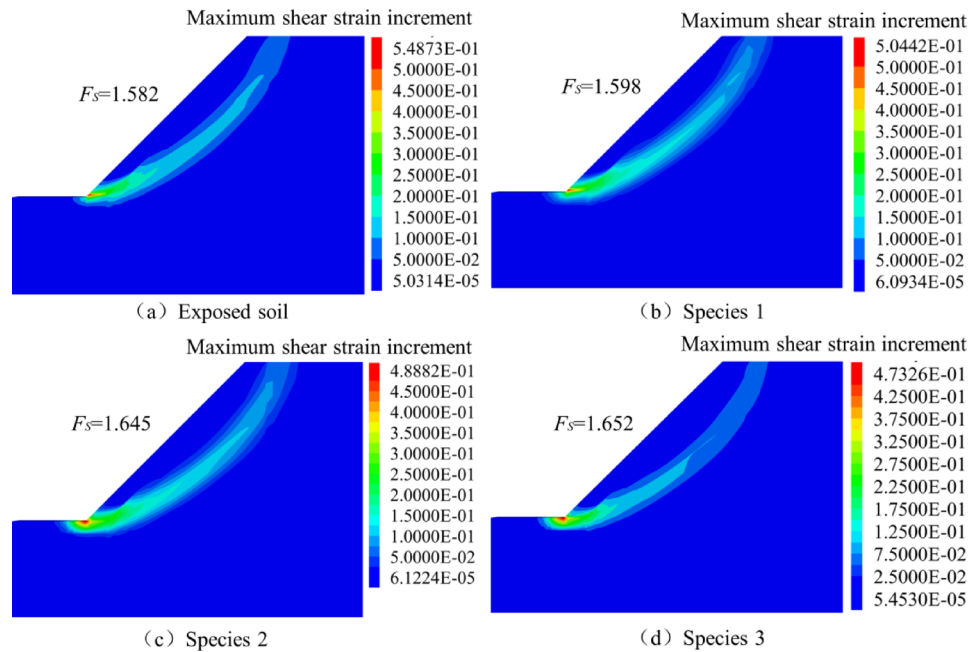


**Fig. 10.** Cloud diagram of the maximum shear strain increment during slope instability.

- in the FBM model, and the FBM model was significantly superior to the Wu model; the root area ratio and the additional cohesive force of the root system were both reduced with the increase of the depth gradually; The increment of the additional cohesive force of root system after Wu model correction was closest to FBM model for Species 1, followed by Species 3, and the furthest difference was for Species 2 root system;
- (3) Mechanical and morphological properties of Species 3 gave its root system the most significant effect on soil consolidation compared to Species 1 and Species 2 root-soil interactions;
  - (4) After implanting the root system on the slope, the upper-stress concentration phenomenon on the circular slip surface of the slope was improved, with the best improvement in the shallow slope of Species 3.

### Data availability

Data availability statement: The datasets used and/or analysed during the current study available from the corresponding author on reasonable request.

Received: 17 November 2024; Accepted: 27 June 2025

Published online: 10 July 2025

### References

1. Wu, H. Atmosphere-plant-soil interactions: theories and mechanisms. *Chin. J. Geotech. Eng.* **39** (01), 1–47 (2017).
2. Zhou, Y., Chen, J. & Wang, X. Progress of study on soil reinforcement mechanisms by root and its expectations. *Ecol. Environ. Sci.* **21** (06), 1171–1177 (2012).
3. Waldron, L. J. The shear resistance of Root-Permeated homogeneous and stratified soil. *Soil Sci. Soc. Am. J.* **41** (5), 843–849 (1977).
4. Wu, T. H., Mickinnell, I. I. W. P. & Swanston, D. N. Strength of tree-roots and landslides on Prince of Wales, Alaska. *Can. Geotech. J.* **1979**, **16**(1):19–33.
5. Natasha, P. & Andrew, S. Estimating the mechanical effects of riparian vegetation on stream bank stability using a fiber bundle model. *Water Resour. Res.*, **41** (7) (2005).
6. Mao, Z. et al. Engineering ecological protection against landslides in diverse mountain forests: choosing cohesion models. *Ecol. Eng.* **45** (2012).
7. Schwarz, M., Cohen & D. Root-soil mechanical interactions during pullout and failure of root bundles. *J. Geophys. Research: Earth Surf.* **115** (F4), F040351–F0 (2010).
8. Zhao, Y. et al. Shear test of plant Root-Soil complex and present status and its mechanical model. *Soil. Water Conserv. China* **403**(10), 51–55 (2015).
9. Zhu, J. et al. Analyses on root reinforcement mechanism based on plant growth process and parameters optimization of Wu model. *Scientia Silvae Sinicae.* **54** (04), 49–57 (2018).
10. Lu, H. et al. In-situ shearing test on the shear strength of soil slope reinforced by plant roots in cold and arid environments. *Chin. J. Rock Mech. Eng.* **35** (08), 1712–1721 (2016).
11. Zhang, Q. et al. Mechanical properties of shrubs and applicability of model WU in karst Ara. *J. Yangtze River Sci. Res. Inst.*, **37**(12), 53–58 (2020).
12. Zhu, J. et al. Analysis of root system enhancing shear strength based on experiment and model. *Rock. Soil. Mech.* **35** (02), 449–458 (2014).
13. Li, B. et al. Study on tensile properties of root-soil composite of alpine meadow plants in the riparian zone of the yellow river source region. *Chin. J. Rock Mech. Eng.* **39** (02), 424–432 (2020).
14. Sui, Z. & Yi, W. Root-reinforced soil mechanics model based on the Griffith fracture criterion. *J. Cent. South. Univ. Forestry Technol.*, **41** (06): 167–174 (2021).

15. Liu, X., Hao, G. & Yu, B. Effect of herb plant root system on the reinforcement of opencast mine dump. *J. Yangtze River Sci. Res. Inst.* **39** (05), 83–88 (2022).
16. Chen, C. et al. Numerical study of effect of roots morphology on shallow stability of slope. *J. Yangtze River Sci. Res. Inst.* **34** (04), 126–130 (2017).
17. Kokutse, N. K. & Temgoua, A. G. T. Slope stability and vegetation: conceptual and numerical investigation of mechanical effects. *Ecol. Eng.* **86**, 146–153 (2016).
18. Yang, Y. et al. The investigation and 3D numerical simulation of herb roots in reinforcing soil and stabilizing slope. *KSCE J. Civil Eng.*, **22**(12): 4909–4921 (2018).
19. Zhao, L. & Zhang, B. Experimental study on root bio-mechanics and relevant factors of *Medicago sativa* and *Digitaria sanguinalis*. *Trans. CSAE.* **23** (9), 7–12 (2007).
20. Shi, C. et al. Effects of roots of *Iris lactea* pall. Var. *Chinensis*(Fisch.) Koidz on soil reinforcement and slope protection. *J. Salt Lake Res.* **30** (3), 98–106 (2022).
21. Hu, J. et al. Straight root tensile properties of *Salix psammophila* in response to Cyclic loading. *ARID Zone Res.* **39** (03), 900–907 (2022).
22. Hao, G. *Study on the Influence of Herbs in Different Growth Periods on the Stability of Shallow Slopes* (Liaoning Technical University, 2022).
23. Liu, X. et al. Study on improvement effect of herb plants on slope stability of dumping site. *J. Saf. Sci. Technol.* **17** (09), 103–108 (2021).
24. Long, H. et al. Study on the influences of the fractal dimension of the root system and slope degree on the slope stability. *Sci. Rep.* **13**(1), 10282–10282 (2023).
25. Yu, D. et al. An experimental study on the pullout mechanical property of tortuous roots manufactured from 3D printing. *Hydrogeol. Eng. Geol.* **51** (1), 82–90 (2024).

### Author contributions

General scientific supervision of work S.; formulation of the research goals and aims, data analysis, and paper preparation; performing experiments, methodology development, data analysis, and preparation of the initial draft G. X. and T. is in charge of processing pictures. All authors have read and agreed to the published version of the manuscript.

### Declarations

### Competing interests

The authors declare no competing interests.

### Additional information

**Correspondence** and requests for materials should be addressed to G.X.

**Reprints and permissions information** is available at [www.nature.com/reprints](http://www.nature.com/reprints).

**Publisher's note** Springer Nature remains neutral with regard to jurisdictional claims in published maps and institutional affiliations.

**Open Access** This article is licensed under a Creative Commons Attribution-NonCommercial-NoDerivatives 4.0 International License, which permits any non-commercial use, sharing, distribution and reproduction in any medium or format, as long as you give appropriate credit to the original author(s) and the source, provide a link to the Creative Commons licence, and indicate if you modified the licensed material. You do not have permission under this licence to share adapted material derived from this article or parts of it. The images or other third party material in this article are included in the article's Creative Commons licence, unless indicated otherwise in a credit line to the material. If material is not included in the article's Creative Commons licence and your intended use is not permitted by statutory regulation or exceeds the permitted use, you will need to obtain permission directly from the copyright holder. To view a copy of this licence, visit <http://creativecommons.org/licenses/by-nc-nd/4.0/>.

© The Author(s) 2025